ACS NANO

www.acsnano.org

Article

Nanoscale Mechanics of FnBPB-Mediated Adhesion of *Staphylococcus aureus* to Skin Ligands

Zhiyong Zheng,[#] Manon Dechene-Tempier,[#] Telmo O. Paiva, Can Wang, Sophie Dunn, Julianne Clowry, Alan D. Irvine, Joan A. Geoghegan,[*] and Yves F. Dufrêne[*]

Cite This: *ACS Nano* 2026, 20, 7279–7290

Read Online

ACCESS | Metrics & More | Article Recommendations | Supporting Information

ABSTRACT: *Staphylococcus aureus* commonly colonizes human skin, impairing barrier integrity and increasing the risk of diseases such as atopic dermatitis (AD). The staphylococcal fibronectin-binding protein B (FnBPB) engages in attachment to the skin, yet little is known about the interaction mechanisms of its two functional regions: an N-terminal A domain responsible for fibrinogen-specific binding, and a C-terminal domain composed of fibronectin-binding repeats (FnBRs). Here, we combine atomic force microscopy with the use of isogenic *S. aureus* strains expressing wild-type FnBPB or domain-specific mutants to dissect the individual contributions of the A domain and FnBRs to two key skin ligands, fibrinogen (Fg) and fibronectin (Fn). Force spectroscopy with bacterial probes reveals that both functional regions play critical roles in mediating the adhesion of *S. aureus* to healthy and AD corneocytes. Force spectroscopy with Fg- or Fn-functionalized tips shows that FnBPB binds Fg via a stress-activated dock, lock, and latch (DLL) mechanism, with forces up to ∼2 nN, while Fn engages in both weak bonds (∼0.1 nN) and strong, force-dependent tandem β-zipper interactions (∼0.8 nN). In the absence of FnBRs, the lifetime and stability of Fg bonds are greatly reduced, suggesting this domain contributes to the bond stability. In addition, the A domain not only governs Fg DLL interaction but also assists Fn-binding. Collectively, our findings provide a biophysical foundation for the multifunctional adhesion properties of FnBPB during skin colonization, being able to bind multiple ligands using a complex synergy of interactions.

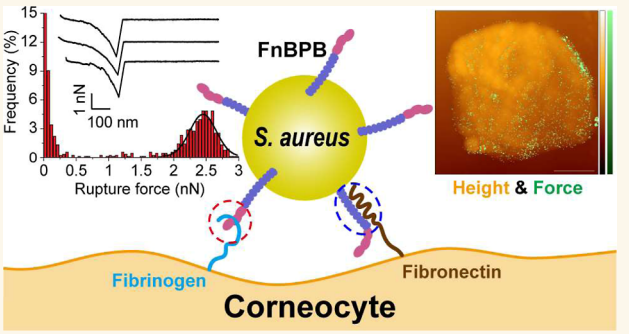

KEYWORDS: *nanoscale adhesion, single-molecules, Staphylococcus aureus, fibronectin-binding protein B, skin, atopic dermatitis*

Staphylococcus aureus is a leading cause of skin and soft tissue infections,[1] whose pathogenicity is intricately tied to the nanoscale interactions at the host–pathogen interface. A hallmark of *S. aureus* is the preferential colonization of disrupted or compromised microenvironments, particularly in atopic dermatitis (AD), a chronic inflammatory skin disorder marked by impaired epidermal barrier integrity, aberrant immune responses, and microbial dysbiosis.[2−4] Central to this colonization is the adhesion of *S. aureus* to host molecules in the stratum corneum (SC), namely, the tight adhesion of *S. aureus* to corneocytes on the outermost surface of the SC,[5,6] and adhesion to the plasma proteins fibrinogen (Fg) and fibronectin (Fn) that exude into the SC as a result of vascular leakage.[7] Cell wall-anchored proteins,[8,9] including fibronectin-binding protein B (FnBPB)[5,6,8] mediate bacterial adhesion to the SC.

FnBPB contains two distinct domains: an N-terminal A domain (domains N1−N3) responsible for binding to corneocyte ligands such as loricrin,[6] corneodesmosin (CDSN),[5,10] and Fg, and a C-terminal segment composed of fibronectin-binding repeats (FnBRs) that bind host Fn (Figure 1a).[8] These distinct domains allow FnBPB to bind multiple specific ligands *in vivo*.[5,6,11,12] FnBPB binds to loricrin on healthy corneocytes,[6] while it has been suggested that the genes encoding loricrin are down-regulated in AD corneocytes,[11,13,14] making loricrin less accessible for binding. In contrast, CDSN is more accessible to *S. aureus* on AD corneocytes than on healthy ones.[5,12] While recent studies have focused on interactions of *S. aureus* with cornified envelope proteins and components such as CDSN, we know less about how interactions with plasma proteins in the SC facilitate *S. aureus* adhesion. A recent study demonstrated that Fg and Fn are among the most abundant plasma proteins in the SC of AD skin, and are also found in healthy skin, albeit less frequently and at lower abundance.[15]

Human Fg is a large, multidomain plasma glycoprotein (∼340 kDa) that plays a pivotal role in hemostasis and wound

Received: December 12, 2025
Revised: February 5, 2026
Accepted: February 6, 2026
Published: February 19, 2026

https://doi.org/10.1021/acsnano.5c21776
ACS Nano 2026, 20, 7279−7290

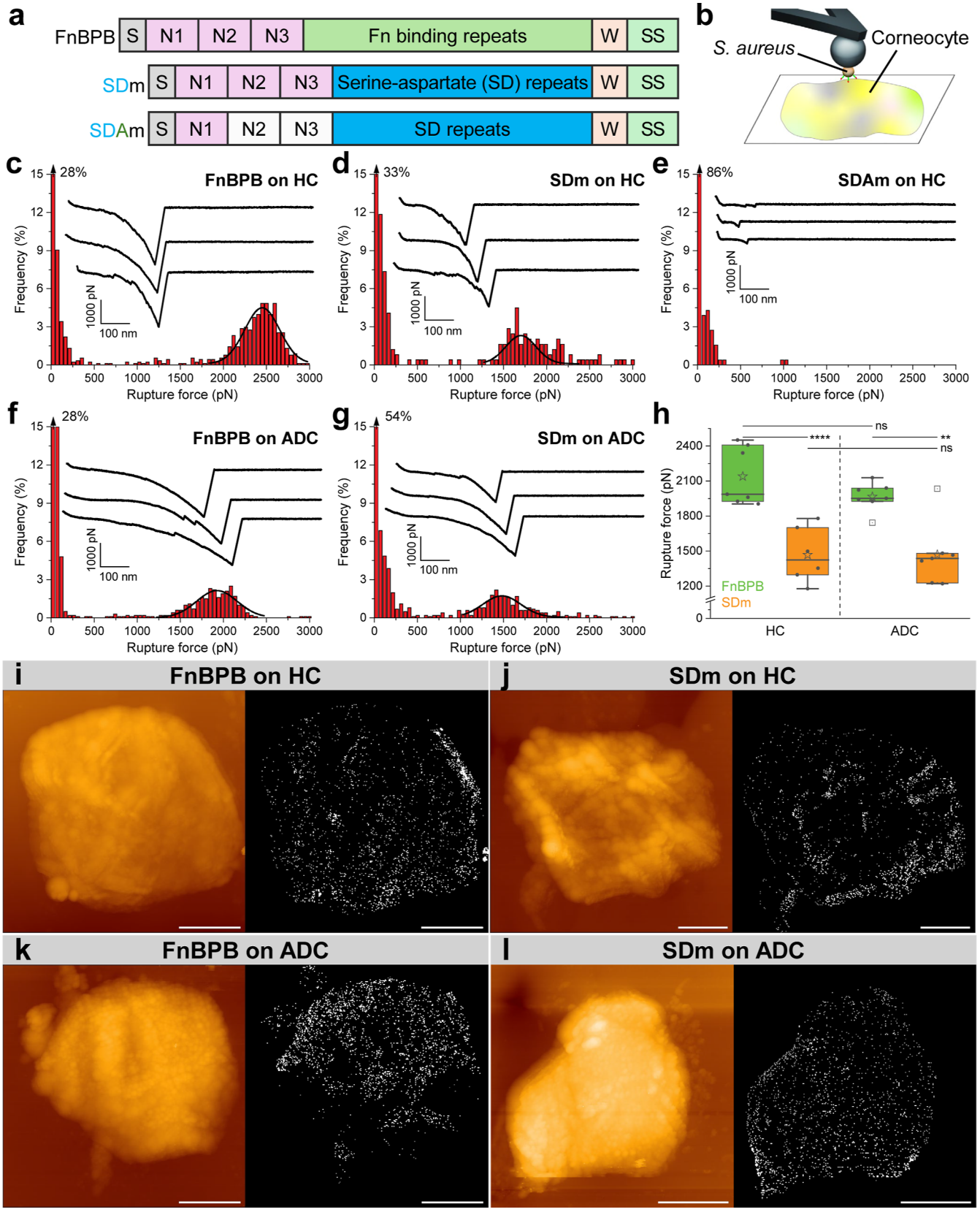

Figure 1. Single-cell force spectroscopy reveals that both the FnBPB A domain and FnBRs enable the adhesion of *S. aureus* to healthy corneocytes (HC) and AD corneocytes (ADC). (a) Schematic diagram showing the domain organization of FnBPB and its variants used in the current study. S: signal sequence; W: wall spanning region; SS: sorting signal. (b) Scheme of single-cell force spectroscopy (SCFS) experiments. (c–g) Representative force-volume rupture force histograms of (c) FnBPB, (d) SDm, and (e) SDAm bacteria interacting with HC, as well as (f) FnBPB and (g) SDm cells interacting with ADC. Insets display three representative retraction force curves. Additional histograms for the adhesion of *S. aureus* to corneocytes are shown in Figures S1 and S2. (h) Boxplots of adhesion force for FnBPB and SDm cells probing HC or ADC. Stars indicate

https://doi.org/10.1021/acsnano.5c21776
ACS Nano 2026, 20, 7279–7290

Figure 1. continued

the mean values, lines the medians, boxes the 25−75% quartiles, whiskers the SD, and open squares the outliers. *P*-values were determined by a one-way ANOVA with a Šidák multiple comparison test to compare variances and are denoted as $^{**}P \leq 0.01$ and $^{****}P \leq 0.0001$, ns: not significant. Quantitative imaging (QI) of (i) FnBPB and (j) SDm cells probing HC, and (k) FnBPB and (l) SDm cells probing ADC. Height (z-range: 5 μm) and adhesion maps (force range: 500 pN) are presented on the left and right, respectively. Scale bar: 10 μm.

healing.[16] Structurally, it consists of two monomers, each comprising three pairs of peptide chains (Aα, Bβ, and γ), forming a symmetrical, elongated molecule ∼85 nm in length.[17] Several staphylococcal adhesins have been shown to bind Fg through the dock, lock, and latch (DLL) mechanism (or its variations), including SdrG,[18,19] ClfA,[20] and SpsD.[21] Following insertion of a short peptide sequence of Fg into a hydrophobic trench formed between the N2 and N3 subdomains of the adhesins, a conformational change at the C-terminus of N3 locks the peptide in place, resulting in a bond that is remarkably resistant to mechanical tension. Several reports have shown that Fg-mediated DLL interactions exhibit a catch-bond behavior, in which the mechanical strength and lifetime of the bonds increase in response to physical stress.[18,20−22] While FnBPB has been suggested to engage in DLL interactions,[23,24] the force and dynamics of this interaction have never been explored.

Fn is a large glycoprotein (∼440 kDa; contour length 120−160 nm) that circulates as a soluble dimer in plasma and other biological fluids but assembles into fibrillar or reticular multimers in the extracellular matrix.[8,25] Each Fn monomer comprises tandem repeats of three homologous modules (FnI, FnII, and FnIII), with two monomers linked head-to-tail via disulfide bonds. The β-sandwich architecture of the FnI and FnIII modules gives rise to the characteristic sawtooth force−distance signatures observed in single-molecule unfolding experiments.[26−28] Fn engages with FnBPB and other related adhesins through a tandem β-zipper mechanism, in which intrinsically disordered FnBRs transition into ordered β-strands upon molecular recognition of FnI.[8,29−32] These β-strands integrate into existing β-sheets of the FnI, forming a reinforced β-sheet architecture that stabilizes the FnBPB-Fn binding.[8,29] Additionally, FnI was also reported to bind the A domain of FnBPB by a different mechanism than the β-zipper,[23] and one of the Fn binding sites is close to the Fg binding site for FnBPA, a close relative of FnBPB.[29,33] Therefore, there is an urgent need to better understand the specific roles and mechanical strengths of the A domain and FnBRs of FnBPB in binding to Fg and Fn in the SC.

In this study, we used atomic force microscopy (AFM) to unravel the nanomechanical forces driving the FnBPB-mediated adhesion of *S. aureus* to the skin ligands Fg and Fn. By interrogating isogenic *S. aureus* strains expressing wild-type FnBPB or domain-specific mutants, we dissected the individual contributions of the A domain and FnBRs and the strength and dynamics of these interactions. We found that FnBPB exhibits two stress-dependent mechanisms, reminiscent of DLL for Fg and tandem β-zipper for Fn. The A domain was also shown to contribute to Fn-binding, via a previously undescribed mechanism. These findings demonstrate that FnBPB forms mechanically tunable nanoscale bridges with two universal epidermal ligands, with force-enhanced binding modalities enabling efficient staphylococcal colonization under physiological shear stress, a pathoadaptive mechanism particularly relevant in the SC in AD.

RESULTS AND DISCUSSION

The FnBPB A Domain and FnBRs Play Critical Roles in Mediating the Adhesion of *S. aureus* to Healthy and AD Corneocytes

To study FnBPB in the absence of other major adhesins, we used a *S. aureus* mutant deficient in ClfA, ClfB, FnBPA, and FnBPB (SH1000 4×) carrying full-length FnBPB on a plasmid (4×) (Table S1). To dissect the roles of the two functional domains in binding to the SC, two mutants were studied: (i) SDm, in which the FnBRs were replaced with serine-aspartate (SD) repeats from ClfA, and (ii) SDAm, in which the key amino acids reported to participate in the binding of the N2N3 domains to Fg (N277, F279) were substituted with alanine (Figure 1a) on the base of SDm (Table S1). SD repeats were employed as flexible spacers to preserve the orientation of FnBPB and preclude steric constraints, which would not be the case if a variant featuring a complete deletion of FnBRs was used.

By means of single-cell force spectroscopy (SCFS),[34] we quantified the interaction forces between these strains and corneocytes obtained by tape-stripping the SC of healthy (HC) or AD (ADC) donors (Figure 1b). Single *S. aureus* bacteria were immobilized onto AFM colloidal cantilevers,[35] and multiple force−distance curves were recorded between the bacterial cantilevers and skin samples immobilized on tape strips, in the force volume mode. Analyzing force−distance curves yielded rupture forces (bond strengths), rupture lengths (extension at which the complex ruptures), and binding frequencies (the percentage of curves showing specific binding events) (Figures 1c−h and S1). For the FnBPB-HC system, most curves featured well-defined and extremely strong adhesion forces of 2139 ± 247 pN (mean ± SD; total of n = 1800 adhesive curves from 7 bacterium−corneocyte pairs, Figure 1c), which are typical of DLL binding forces.[18,36] Binding of SDm to HC was characterized by forces that were also very large, 1467 ± 237 pN (n = 1125 adhesive curves; 6 bacterium−corneocyte pairs, Figure 1d), yet weaker than for FnBPB (Figure 1h), pointing to the importance of FnBRs in securing ultrastrong adhesion. This phenomenon could mean that the FnBRs region functions as a spacer ensuring optimal exposure and orientation of the A domains for proper DLL interactions, or that the FnBRs region itself is essential. By contrast, binding of SDAm to HC showed weaker forces, while strong forces (>1 nN) were almost abolished (Figure 1e), and thus this strain was not further characterized by SCFS. These data show that the A domain and FnBRs play a direct role in the strong adhesion to corneocytes in the healthy SC.

We asked whether the adhesion of FnBPB and SDm strains to ADC differs from that of HC. Forces of 1964 ± 121 pN (n = 2838 adhesive curve; 7 bacterium−corneocyte pairs) and 1468 ± 272 pN (n = 4925 adhesive curve; 7 bacterium−corneocyte pairs) were recorded for FnBPB and SDm, respectively (Figures 1f,g and S2). Figure 1h summarizes the rupture forces of FnBPB and SDm to HC or ADC, and similar trends are observed: the rupture force of FnBPB strain is larger

https://doi.org/10.1021/acsnano.5c21776
ACS Nano 2026, 20, 7279−7290

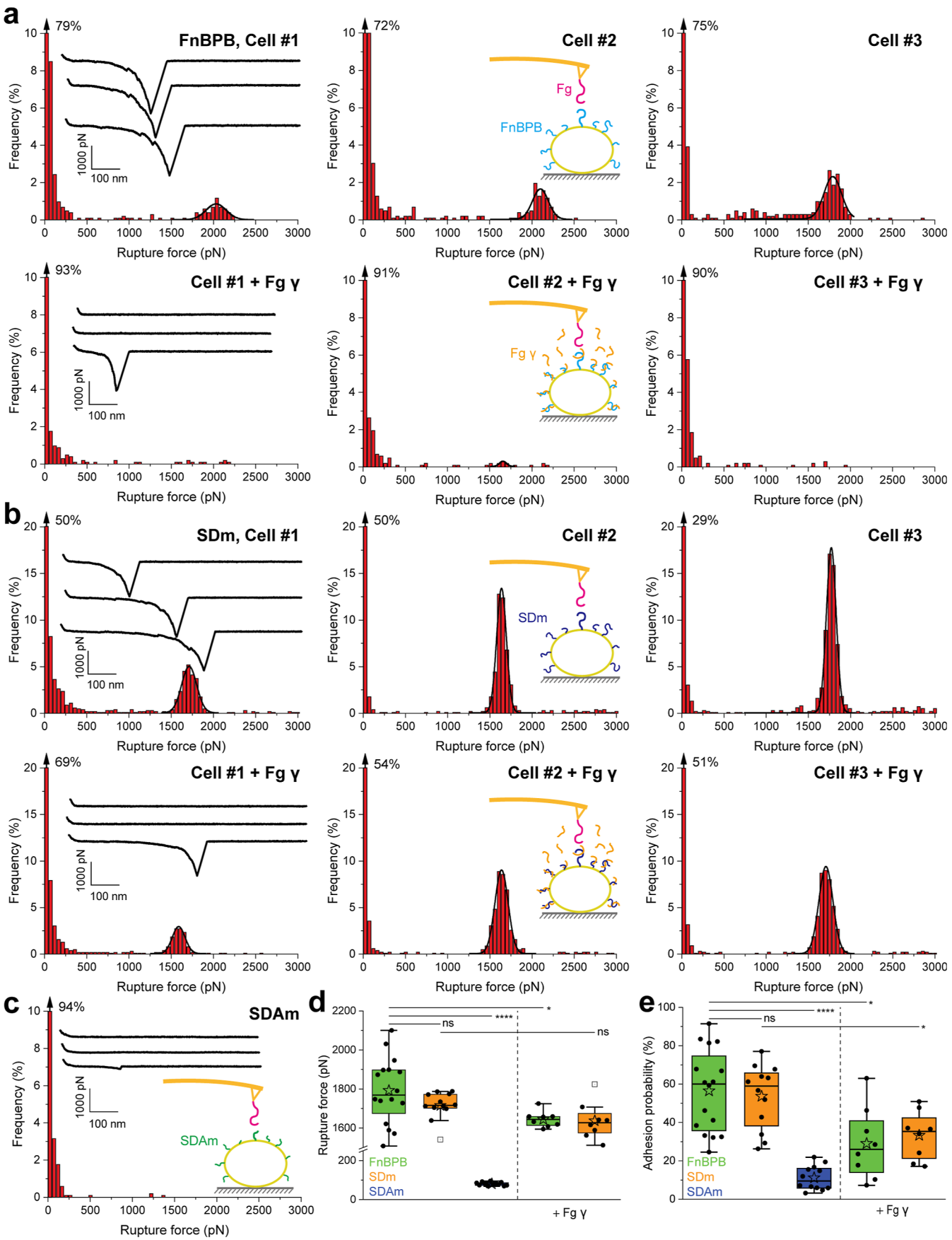

Figure 2. Single-molecule force spectroscopy demonstrates that the FnBPB A domain binds fibrinogen (Fg) with ultrastrong DLL forces that do not depend on the FnBRs. Representative histograms of rupture forces obtained with Fg-tips for (a) FnBPB and (b) SDm (upper) before and (lower) after the Fg γ-chain C-terminal peptide (100 μg mL^{-1}) was injected. Insets: three representative retraction force curves. (c) Rupture force

https://doi.org/10.1021/acsnano.5c21776
ACS Nano 2026, 20, 7279−7290

Figure 2. continued

histograms of Fg-tips probing SDAm. Corresponding histograms of rupture length are shown in Figure S4. Corresponding boxplots of (d) rupture force and (e) adhesion probability of FnBPB and SDm before and after the incubation with Fg γ-chain C-terminal peptide. Stars indicate the mean values, lines the medians, boxes the 25−75% quartiles, whiskers the SD, and open squares the outliers. *P*-values were determined by a one-way Brown-Forsythe and Welch ANOVA test with a Dunnett T3 multiple comparison test to compare variances and are denoted as $^{*}P \leq 0.05$, $^{****}P \leq 0.0001$, and ns: not significant.

than that of SDm strain when they bind to HC or ADC. However, there was no substantial difference between the rupture force of FnBPB strain binding to HC and ADC, likewise for SDm. Finally, rupture length histograms obtained for FnBPB and SDm bacteria interacting with HC and ADC cells featured a wide range of extensions (from ∼25 to ∼600 nm), suggesting that different types of interactions were at play.

To investigate the spatial distribution of binding events on the corneocyte surfaces, SCFS in the quantitative imaging (QI) mode was used,[37] in which bacterial cantilevers scan across the whole surface of corneocytes at high speed to acquire high-resolution images of topography and adhesion. Adhesion maps revealed heterogeneously distributed adhesion events for all pairs of bacterium-corneocyte, i.e., for FnBPB and SDm strains as well as HC and ADC (Figure 1i−l). As previously reported,[2,38] adhesion microdomains of ligands have been observed on the surface of corneocytes, with their distribution predominantly localized at the cell periphery. However, further investigation is required to elucidate the microdomain molecular origin and functional significance. We also note that the adhesion force magnitudes followed the same trend as in the force-volume mode (Figure S3).

Fg-Binding by FnBPB is an Ultrastrong DLL Interaction that Mainly Involves the A Domain

As Fg and Fn are two prototypical human proteins that interact with FnBPB,[23,39] and found in the SC of both healthy and AD skin,[15] we dissected the strength and dynamics of these two FnBPB-ligand interactions. We employed single-molecule force spectroscopy (SMFS),[34] in which AFM tips functionalized with Fg or Fn at low density are used to generate multiple force−distance curves across the top area of a single living *S. aureus* cell. Fg-binding to FnBPB was characterized by strong forces of 1792 ± 168 pN (n = 8496 adhesive curves from 16 cells, upper panel of Figure 2a). The binding force is slightly lower than that of FnBPB-HC but comparable to that of FnBPB-ADC. Note that the orientations and accessibility of Fg can differ when attached to the AFM tips compared to the SC surface, leading to some differences in absolute rupture forces.

Adhesin FnBPB is believed to specifically bind to the extreme C-terminus of the Fg γ-chain via a DLL mechanism.[6,24,40] To test whether DLL is involved here, competitive blocking experiments were performed using a short peptide mimicking the Fg γ-chain C-terminal sequence (GEGQQHHLGGAKQAGDV). FnBPB cells were probed with Fg-modified AFM tips before and after peptide injection (Figure 2a). The binding forces remain in the DDL bond range (Figure 2d). However, it significantly decreased the frequencies of strong interactions, from 56.4 ± 21.5% to 29.0 ± 18.8% after injection (n = 2364 adhesive curves from 8 cells treated with Fg γ, Figure 2e), showing that the forces were specific to the FnBPB-Fg interaction. This result, together with the fact that for all cells examined, adhesion forces featured narrow distributions centered around 1.5−2 nN (Figure 2a), which match DLL forces,[6,18,41,42] suggest that single FnBPB-Fg DLL bonds were being probed.

SDm cells were also studied with Fg-modified AFM tips to identify the potential role of FnBRs in the interaction between FnBPB and Fg. As shown in Figure 2b,d, strong rupture forces of 1715 ± 70 pN (n = 6475 adhesive curves from 12 cells) appeared in the Fg bound to SDm, which is akin to that of Fg bound to FnBPB cells. This is consistent with the notion that the N2 and N3 domains are responsible for the DLL binding between Fg and FnBPB,[8] and also indicate that FnBRs are not determinant in the binding to Fg. Blocking experiments showed that Fg γ did not change the magnitude of strong binding forces (Figure 2d), but reduced the frequencies of strong forces from 53.6 ± 16.8% to 37.6 ± 14.5% (12 and 8 cells, respectively, Figure 2e). Strong adhesion forces completely vanished for the Fg-SDAm interaction (n = 1352 adhesive curves from 12 cells, Figure 2c−e), which further confirms the role of N2 and N3 subdomains of FnBPB in DLL binding. These results show that a DLL mechanism is involved in the very strong interaction between Fg and the FnBPB N2 and N3 domains, while FnBRs do not seem to play a crucial role.

Both FnBRs and the A Domain Participate in Fn-Binding

The binding strength of *S. aureus* to Fn was then quantified by SMFS using Fn-functionalized tips (Figure 3). The FnBPB strain showed an average rupture force of 75 ± 29 pN (n = 2350 adhesive curves from 7 cells, Figure 3a), SDm averaged 55 ± 12 pN (n = 1849 adhesive curves from 7 cells, Figure 3b), and SDAm averaged 71 ± 24 pN (n = 1946 adhesive curves from 9 cells, Figure 3c). Hence, the three strains showed comparable rupture forces. The adhesion probabilities were also calculated (Figure 3f). FnBPB cells showed an average adhesion probability of 32.8 ± 9.1%, while SDm and SDAm displayed a reduced adhesion probability of 15.4 ± 7.4% and 16.9 ± 10.8%, respectively. Conversely, adhesion virtually vanished on the 4× mutant, a mutant strain transformed with an empty plasmid lacking the gene encoding FnBPB, which showed an average adhesion probability of 1.9 ± 1.7% (5 cells, Figure 3d). Since the 4× mutant strain featured no adhesion, one can conclude that the rupture events observed on the other three strains (FnBPB, SDm, and SDAm strains) reflect specific binding.

Adhesion forces >800 pN were also seen for the FnBPB strain (Figure 3e, left panel), sometimes with sawtooth patterns (Figure 3e, right panel), while they were hardly observed on SDm and SDAm. These profiles are reminiscent of the so-called tandem β-zipper mechanism reported previously for the interaction between FnBPA and Fn,[43] where multiple FnBRs sequentially engage with Fn, progressively strengthening the adhesion force.

A decrease of approximately 50% in adhesion probability was observed between FnBPB cells (32.8 ± 9.1%) and SDm cells (15.4 ± 7.4%), indicating that roughly half of the adhesion events of the FnBPB strain are generated by the

https://doi.org/10.1021/acsnano.5c21776
ACS Nano 2026, 20, 7279−7290

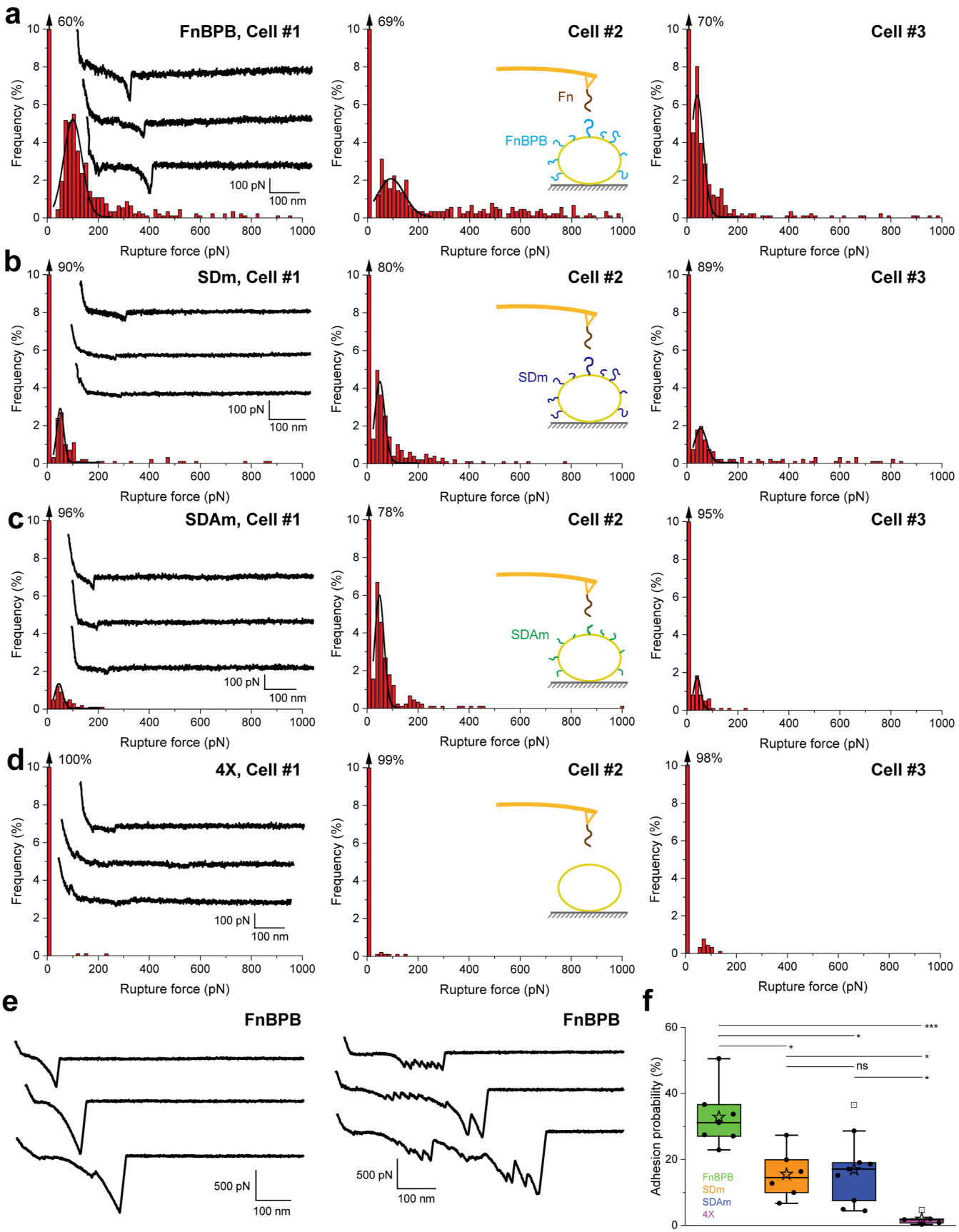

Figure 3. Single-molecule force spectroscopy reveals the role of the A domain and FnBRs in the adhesion of *S. aureus* to fibronectin (Fn). Representative histograms of rupture forces for the interaction between Fn-tips and (a) FnBPB, (b) SDm, (c) SDAm, and (d) the strain carrying empty plasmid (4×). Insets: three representative retraction curves. Corresponding histograms of rupture length are shown in Figure S5. (e) Representative curves of the strong β-zipper interaction observed on the FnBPB strain. (f) Corresponding boxplots of adhesion probability of

https://doi.org/10.1021/acsnano.5c21776
ACS Nano 2026, 20, 7279−7290

Figure 3. continued

FnBPB, SDm, SDAm, and 4× strains. Stars indicate the mean values, lines the medians, boxes the 25−75% quartiles, whiskers the SD, and open squares the outliers. *P*-values were determined by a one-way Brown-Forsythe and Welch ANOVA test with a Dunnett T3 multiple comparison test to compare variances and are denoted as $*P \leq 0.05$, $***P \leq 0.001$, and ns: not significant.

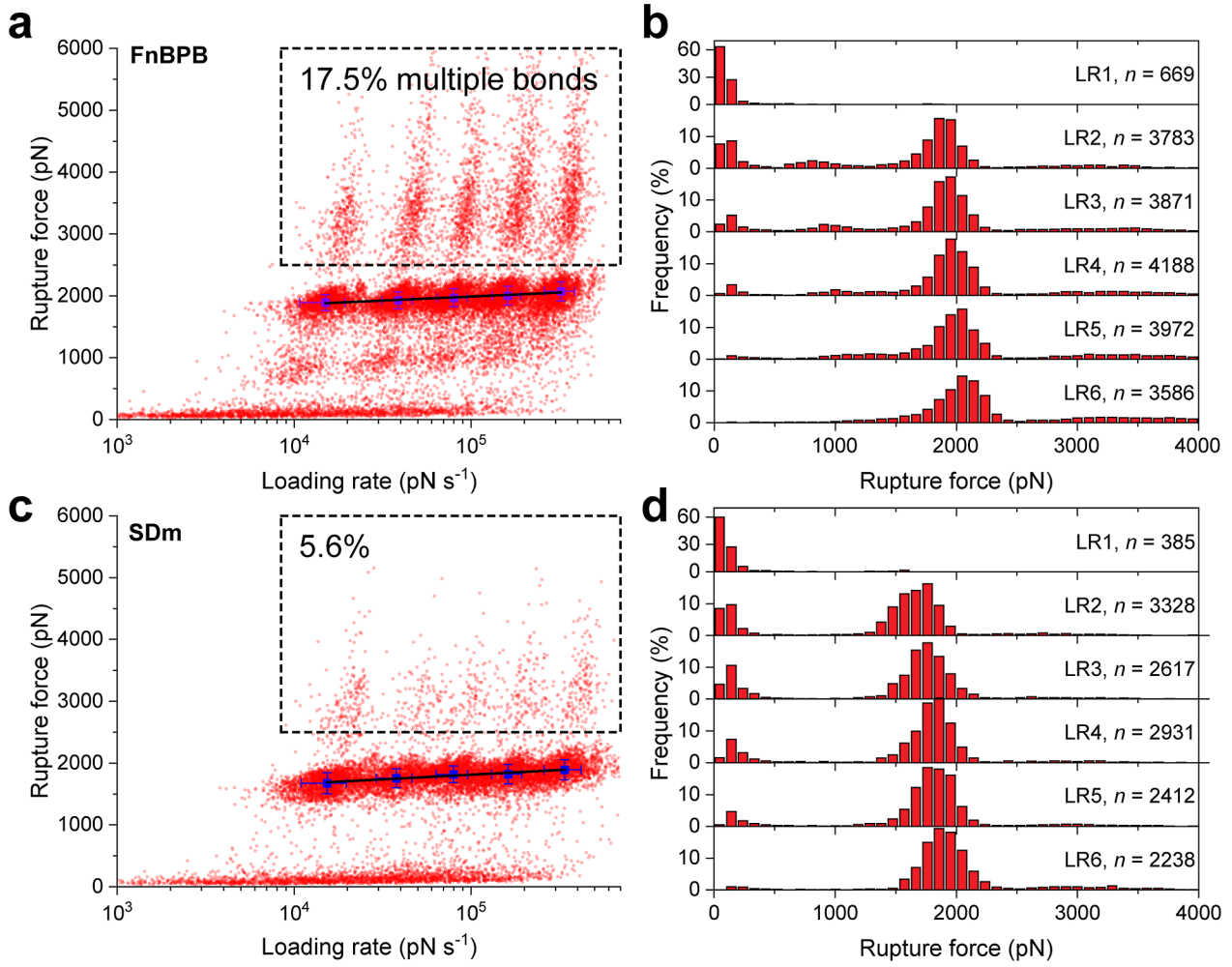

Figure 4. Force-induced strengthening of the interaction between FnBPB and Fg. Dynamic force spectroscopy (DFS) plot of rupture force vs loading rate of (a) FnBPB (n = 20,072 data points; 7 cells) and (c) SDm (n = 13,966 data points; 8 cells). The solid lines show the extrapolated Bell-Evans fit through the most probable (mean) rupture forces and loading rates for five loading rate (LR) bins shown as solid squares. Error bars are the standard deviations. Bell−Evans model yielded $k_{off} = 9.25 \times 10^{-13}$ s^{-1} and $x_\beta = 0.073$ nm for FnBPB, the complex off-rate constant and distance along the reaction coordinate of the transition between bound and unbound states, respectively. For SDm, $k_{off} = 1.39 \times 10^{-9}$ s^{-1} and $x_\beta = 0.063$ nm. The frequency of adhesion events with strong force (>2.5 nN) is much higher on FnBPB cells (17.5%) than SDm (5.6%), as shown in the dashed line squares. Corresponding histograms and Gaussian fits of (b) FnBPB and (d) SDm. The discrete LR ranges are $1 \times 10^3 <$ LR1 $< 6 \times 10^3$, $6 \times 10^3 \leq$ LR2 $< 2.4 \times 10^4$, $2.4 \times 10^4 \leq$ LR3 $< 5.4 \times 10^4$, $5.4 \times 10^4 \leq$ LR4 $< 1.12 \times 10^5$, $1.12 \times 10^5 \leq$ LR5 $< 2.25 \times 10^5$, $2.25 \times 10^5 \leq$ LR6 $< 5.7 \times 10^5$ pN s^{-1}. The values of n indicate the number of adhesion events.

FnBRs, whereas the other half involves the A domain. The majority of the adhesion events for the SDm strain were characterized by weak forces, as expected since the DLL mechanism was not involved. The similar adhesion probabilities of the SDAm and SDm strains to Fn (Figure 3f) indicate that the A-domain−Fn interaction involves amino acid residues located outside the primary Fg-binding pocket. This suggests a previously undescribed binding mechanism that warrants further investigation.

Interestingly, there were major differences in rupture lengths for the Fg and Fn complexes (Figures S4 and S5). Bacteria interacting with Fg featured rupture lengths of 443 ± 7 nm (mean ± s.d.; 6 cells) for FnBPB and 456 ± 53 nm (6 cells) for SDm cells, respectively. Assuming that each amino acid contributes 0.36 nm to the contour length of a polypeptide chain, the length of a fully extended FnBPB protein (940 amino acids) is expected to be 338 nm, thus in the range of what we observe. This suggests that pulling on the complex at very high forces leads to the full unfolding of the adhesin. It is very likely that the FnBRs would fully unfold as they are intrinsically disordered.[8] As for the N domains, while they can sustain very high tension, they may unfold (at least partially) before rupture. Note that we must also consider that stretching of the ligands may contribute to the observed extensions, but to a moderate extent, as they were attached to the tips via a multisite chemistry. By contrast, Fn forces featured only short

https://doi.org/10.1021/acsnano.5c21776
ACS Nano 2026, 20, 7279−7290

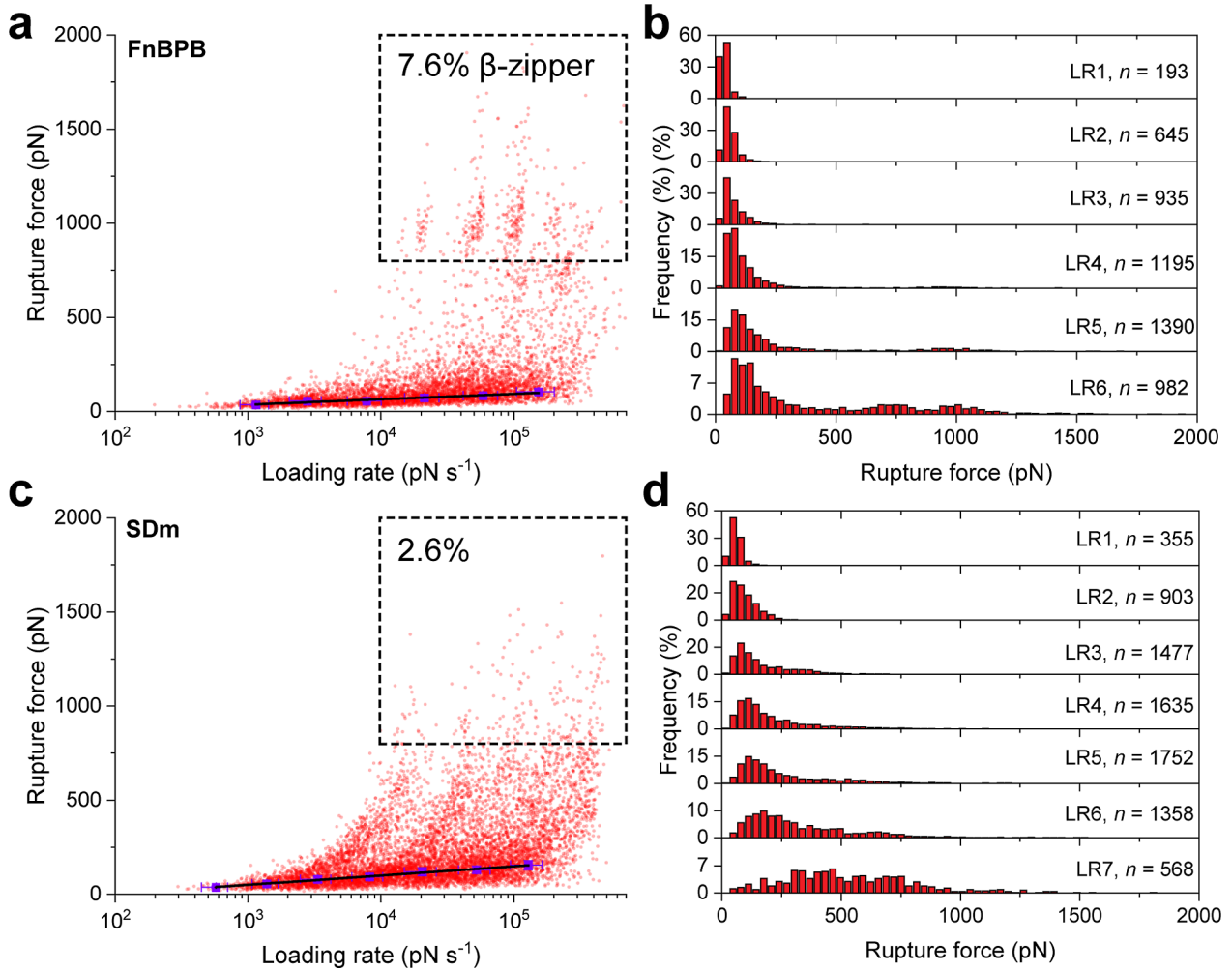

Figure 5. Mechanostability of the interaction between FnBPB and Fn. Dynamic force spectroscopy plot of rupture force vs loading rate of (a) FnBPB strain (n = 5529 data points; 7 cells) and (c) SDm (n = 8078 data points; 6 cells). The solid lines show the extrapolated Bell-Evans fit through the most probable (mean) rupture forces and loading rates (LR) bins shown as solid squares. Error bars are the standard deviations. Bell–Evans model yielded k_{off} = 4.64 s^{-1} and x_β = 0.330 nm for FnBPB strain. For SDm, k_{off} = 4.59 s^{-1} and x_β = 0.191 nm. (b) Corresponding histograms and Gaussian fits of FnBPB strain. The discrete LR ranges are $5.52 \times 10^2 \leq$ LR1 $< 1.54 \times 10^3$, $1.54 \times 10^3 \leq$ LR2 $< 4.31 \times 10^3$, $4.31 \times 10^3 \leq$ LR3 $< 1.21 \times 10^4$, $1.21 \times 10^4 \leq$ LR4 $< 3.37 \times 10^4$, $3.37 \times 10^4 \leq$ LR5 $< 9.42 \times 10^4$, $9.42 \times 10^4 \leq$ LR6 $< 2.63 \times 10^5$ pN s^{-1}. (d) Corresponding histograms and Gaussian fits of SDm, The discrete LR ranges are $7.54 \times 10^2 \leq$ LR1 $< 1.92 \times 10^3$, $1.92 \times 10^3 \leq$ LR2 $< 4.89 \times 10^3$, $4.89 \times 10^3 \leq$ LR3 $< 1.25 \times 10^4$, $1.25 \times 10^4 \leq$ LR4 $< 3.17 \times 10^4$, $3.17 \times 10^4 \leq$ LR5 $< 8.09 \times 10^4$, $8.09 \times 10^4 \leq$ LR6 $< 2.06 \times 10^5$, $2.06 \times 10^5 \leq$ LR7 $< 5.24 \times 10^5$ pN s^{-1}. The values of n indicate the number of adhesion events.

ruptures, 110 ± 52 nm (7 cells), and 53 ± 22 nm (6 cells) for FnBPB and SDm bacteria, respectively, in agreement with the expected, as only the FnBRs, and not the A domain, are elongated under force.

Physical Stress Activates the Ultrastrong FnBPB-Fg Binding Force

Pathogens need to establish firm adhesion to the skin or other surfaces during colonization to prevent detachment by various physical stresses, such as cell surface contact and hydrodynamic flow.[44] To accomplish this, bacteria have evolved specialized adhesion strategies that are activated in response to mechanical stress. To test this, we first investigated the effect of applied mechanical tension on the FnBPB–Fg bond by measuring rupture forces while varying the tip-retraction speed, i.e., dynamic force spectroscopy (DFS).[45] Force values were plotted as a function of loading rate (LR), calculated from the linear slope immediately preceding each rupture event on the force vs time curves. For this interaction, weak bonds (<150 pN) were predominantly seen under low *LRs* (<6×10^3 pN s^{-1}), while much stronger bonds (≥1.8 nN) were mainly observed at higher *LRs* from 6×10^3 to 5.7×10^5 pN s^{-1}, Figure 4a,b. This demonstrates that mechanical force activates the FnBPB–Fg interaction, analogous to the DLL force behavior of other Fg-binding adhesins (ClfA, ClfB, and SpsD),[20,21,45] as well as the force-enhanced catch bonds formed by FnBPB–loricrin and other staphylococcal adhesin–ligand pairs.[6,41,46] The high-forces were fitted with the Bell–Evans model, yielding two dissociation kinetic parameters, x_β and k_{off}.[34,47] x_β, the distance between the bound state and the transition state along the reaction coordinate was determined from the slope of the force versus ln(*LR*) plot, while k_{off}, the kinetic off-rate constant of dissociation, was extrapolated to zero force. Values of $k_{off} = 9.25 \times 10^{-13}$ s^{-1} and x_β = 0.073 nm were obtained, falling within the range of those previously determined for the SdrG-Fg complex, $k_{off} = 9.2 \times 10^{-11}$ s^{-1} with x_β = 0.051 nm,[18] known to engage in a DLL interaction. Such a low k_{off} points to an extremely stable and strong

https://doi.org/10.1021/acsnano.5c21776
ACS Nano 2026, 20, 7279–7290

FnBPB-Fg bond under high loads. At *LRs* above 10^4 pN s^{-1}, even much higher forces (2 to 6 nN) were observed, which reflect multiple bonds probed in parallel. It should be noted that rupture forces and kinetic parameters derived from DFS measurements describe the mechanostability of the FnBPB complexes under tension, which may differ from biochemical affinity values determined under equilibrium conditions.

Second, for SDm-Fg, weak bonds (<150 pN) were predominantly seen under low *LRs*, while much stronger bonds (>1.6 nN) were mainly observed at higher *LRs* (Figure 4c,d). Fitting the high−force regime DFS data gives k_{off} = 1.39 × 10^{-9} s^{-1} and x_β = 0.063 nm. The k_{off} is 4 orders of magnitude greater than that measured for the FnBPB−Fg interaction, indicating distinct kinetic profiles: the Fg−SDm mutant bond exhibits a markedly higher off-rate, corresponding to a shorter lifetime and reduced stability. Additionally, as shown in Figure 4, the proportion of rupture events with very strong forces (2.5−6 nN) at *LRs* above 10^4 pN s^{-1}, was higher for FnBPB cells (17.5%) than SDm cells (5.6%). Our SMFS experiments show that FnBRs influence Fg-binding, which is in line with earlier data where amino acid substitutions in the FnBRs region affect binding to Fg.[48] We suggest that the presence of the FnBRs region might enhance the accessibility of the N2N3 domains to their ligand and reinforce bond stability, leading to longer-lived bonds. However, alternative explanations such as changes in the molecular orientation of the adhesin/ligands, the effective length of the linker employed for tip functionalization, and associated steric hindrances or force-loading geometry, cannot be ruled out.

Mechanical Stress Promotes Strong FnBPB-Fn Tandem β-Zipper Interactions

We next evaluated the behavior of the FnBPB-Fn interaction under tensile loading using DFS. At low LRs (<1.21 × 10^4 pN s^{-1}), only weak forces (<100 pN) were predominantly observed. At higher LRs (≥1.21 × 10^4 pN s^{-1}), however, stronger forces (>800 pN) were also seen (Figure 5a,b). We believe these non-DLL strong forces originate from a tandem β-zipper binding mechanism, similar to the behavior reported for the SpsD-Fn bond.[22] Fitting the low−force regime with the Bell−Evans model gives k_{off} = 4.64 s^{-1} and x_β = 0.330 nm. For SDm (Figure 5c,d), weak forces (<150 pN) dominated at low LRs (<3.17 × 10^4 pN s^{-1}), while stronger forces larger than 800 pN appeared at high LRs (≥3.17 × 10^4 pN s^{-1}), yet at a much lower frequency 2.6% vs 7.6% than for FnBPB, thus supporting strongly the notion that these high forces reflect β-zipper interactions. The low-force fitting yielded k_{off} = 4.59 s^{-1} and x_β = 0.191 nm, suggesting FnBPB and SDm form similar weak bounds with short lifetimes.

In summary, our force spectroscopy data point to the roles of the FnBPB A domain and FnBRs interacting with Fg and Fn, especially the effects of the FnBRs on Fg binding and of the A domain on Fn binding. In the future, computational tools[49] would greatly contribute to further dissecting these complex mechanisms at the atomic scale, and to fully characterize the synergistic cooperation between the FnBPB domains.

CONCLUSIONS

FnBPB binds to healthy and AD corneocyte ligands via two distinct functional regions: the N-terminal A domain mainly responsible for fibrinogen-specific binding, and the C-terminal FnBRs. In this work, we have unraveled the molecular forces driving the binding of FnBPB to the two key corneocyte ligands, Fg and Fn. The FnBPB N2N3 domains trigger ultrastrong Fg binding through a DLL mechanism, with forces up to 2 nN, that are activated by physical stress. Replacement of the FnBRs with serine-aspartate repeats strongly increases the dissociation constant of the FnBPB-Fg interaction, compatible with a decrease in the lifetime and stability of Fg bonds, supporting the notion that this domain contributes to the bond stability. The FnBRs region engages in a tandem β-zipper interaction with Fn (>800 pN), which is induced by mechanical tension. Mutational analysis with live cells reveals that the A domain not only governs Fg DLL binding but also assists Fn-binding through a so far poorly understood mechanism. *In vivo*, we speculate that in the healthy stratum corneum, where loricrin is abundant,[6] Fg and Fn serve as additional ligands; in AD skin, where Fg and Fn are more abundant, *S. aureus* FnBPB promotes interaction with these ligands, alongside binding to CDSN.[5] The results emphasize the variety and complexity of FnBPB-binding mechanisms (weak vs strong forces, physical stress activation, multiple ligand specificity, synergistic role of the two adhesin domains), providing a biophysical foundation for its multifunctional adhesion properties, and rationalizing its key role in skin colonization and disease. While the present study focused on the experimental single-molecule exploration of FnBPB interactions, further research integrating computational tools will be essential to provide high-resolution structural validation and deeper atomistic insights into these interactions.[49]

MATERIALS AND METHODS

Bacterial Strains

All strains are described in Table S1. *S. aureus* SH1000 deficient in ClfA, ClfB, FnBPA, and FnBPB (SH1000 4×) (Table S1) was used as the host strain for all plasmids.

Bacterial Growth Conditions

S. aureus derivatives were grown in tryptic soy agar with chloramphenicol (10 μg mL^{-1}) at 37 °C. A single colony was selected and transferred to 10 mL of tryptic soy broth (TSB) supplemented with chloramphenicol (10 μg mL^{-1}) and incubated at 37 °C overnight under continuous agitation (180 rpm). Cultures were washed once with TSB and diluted to an OD_{600} of 0.05 in 10 mL of TSB supplemented with chloramphenicol (10 μg mL^{-1}) and incubated at 37 °C until they reached the exponential phase (OD_{600} of around 0.3). The culture was harvested by 5 min centrifugation at 2000*g* and washed twice with PBS (pH 7.4). The bacterial suspension was then diluted 100 times in PBS for AFM experiments.

Corneocyte Collection

The stratum corneum was sampled using circular adhesive tapes (22 mm diameter D-squame Discs; CuDerm Corporation, USA). The tapes were applied to nonlesional forearm skin of AD patients with concurrent *S. aureus* infection at another body site, and healthy controls as previously described.[50] Adhesive tapes were pressed for 10 s with a pressure of 225 g cm^{-2}, using a D-squame pressure instrument D500 (CuDerm Corporation, USA). Consecutive tape strips were collected from the same skin site and placed individually in 2 mL cryovials and stored at −80 °C. Either the sixth or seventh tape strip was used for all analyses carried out in this study, with strips that had been stored for 3−4 years. No cleaning, washing, or chemical treatment was applied prior to analysis. Corneocyte studies were conducted in accordance with the Declaration of Helsinki and was approved by the Research Ethics Committee of Children's Health Ireland at Crumlin, Dublin, Ireland (GEN-612−17). Written

https://doi.org/10.1021/acsnano.5c21776
ACS Nano 2026, 20, 7279−7290

informed consent from parents/guardians and patient assent (where feasible) was obtained prior to study enrolment.

Single-Cell Force Spectroscopy

Single-cell probes were prepared as described previously.[34,51−53] Tipless cantilevers (NP−O10, Bruker) were mounted on a JPK NanoWizard 3 AFM and brought into contact with a thin film of UV-curable adhesive (NOA 63, Norland Edmund Optics) deposited on a glass slide. Under AFM motor control, individual cantilevers were used to capture single 6.1 μm silica microspheres (Bangs Laboratories) by adhesion to the uncured glue. The assemblies were then exposed to UV light for 20 min to polymerize the adhesive. Colloidal probes were functionalized by immersion in 4 mg mL^{-1} dopamine hydrochloride in Tris-buffered saline (10 mM Tris, 150 mM NaCl, pH 8.5) for 1 h in the dark, followed by three PBS rinses. A diluted bacterial suspension was incubated on a polystyrene Petri dish (TPP 93040) for 20 min to permit cell attachment, after which the dish was gently washed and filled with 3 mL PBS for AFM measurements at room temperature. Cantilever spring constants (~0.06 N m^{-1}) were determined by the thermal-noise method.[54] Individual bacteria were then captured on the colloidal probes under inverted-microscope observation. The bacterial probes were positioned above corneocyte samples (affixed to the dish with double-sided tape), and a 32 × 32-pixel force map (1.5 μm × 1.5 μm) was acquired using a 250 pN force set point, 1 μm s^{-1} approach/retraction speed, 1 μm ramp length, zero dwell time, and closed z-loop control. Quantitative imaging was performed with a 250 pN contact set point, 1 μm ramp length, and 40 μm s^{-1} approach/retraction speed over an area encompassing an entire corneocyte.

Tip Functionalization with Fg or Fn

Gold-coated PNP-TR-Au cantilevers (NanoWorld) were cleaned sequentially by rinsing with deionized water and ethanol, drying under a nitrogen stream, and exposing to UV−ozone (Jelight Co., Irvine, CA) for 15 min. Cleaned cantilevers were then incubated overnight in the dark in a 1 mM ethanolic solution of 16-mercaptododecahexanoic acid and 1-mercapto-1-undecanol (10:90 mol % for Fn functionalization or 1:99 mol % for Fg functionalization). After three ethanol rinses and drying, the cantilevers were activated by immersion in a freshly prepared aqueous solution of *N*-hydroxysuccinimide (NHS, 10 mg mL^{-1}) and 1-ethyl-3-(3-(dimethylamino)propyl)-carbodiimide (EDC, 25 mg mL^{-1}) for 30 min (dark). Following a rinse in ultrapure water, cantilevers were incubated for 1 h in PBS containing 0.1 mg mL^{-1} Fg (Abcam) or Fn (Merck Millipore). Finally, functionalized cantilevers were rinsed in PBS and stored at 4 °C in PBS until use.

Single-Molecule Force Spectroscopy

A 200 μL suspension of bacteria diluted in PBS was deposited onto a polystyrene Petri dish and incubated for 20 min to permit cell attachment. The dish was then gently rinsed twice with PBS and refilled with 3 mL PBS for AFM measurements. All experiments were performed at room temperature on a JPK NanoWizard 3 NanoScience AFM. Cantilever spring constants (0.037−0.048 N m^{-1}) were determined via the thermal-noise method. Force−distance curves were acquired in force-volume mode with a 250 pN force set point, 1 μm s^{-1} approach and retraction speed, 1 μm ramp length, zero dwell time, and closed z-loop. For force maps, 32 × 32 pixels were recorded over a 500 × 500 nm^2 area atop an individual bacterium. Blocking assays involved recording force maps on the same cell before and 15 min after the addition of 100 μg mL^{-1} γ-chain fibrinogen peptide (Genscript). In dynamic force spectroscopy (DFS) measurements, all parameters were held constant except retraction speeds, which were varied at 1, 2.5, 5, 10, and 20 μm s^{-1}. The final rupture event in each curve was fitted to the worm-like chain model of polymer extension to extract the rupture force, rupture length, and loading rate.

Statistics and Reproducibility

Statistical analyses were conducted using OriginPro 2021. Binding-frequency and force differences were evaluated one-way ANOVA tests with exact p-value ranges reported in the figure captions. Single-bond rupture events in dynamic force spectroscopy were fitted to the Bell−Evans model. Sample sizes, biological replicates, and technical .replicates are detailed in both the main text and figure legends.

■ ASSOCIATED CONTENT

Supporting Information

The Supporting Information is available free of charge at https://pubs.acs.org/doi/10.1021/acsnano.5c21776.

The details of the strains used in this study; additional rupture force and rupture length data of the SCFS of *S. aureus* cells probing corneocytes; rupture length data of the SMFS of *S. aureus* cells probed by Fg and Fn (PDF)

■ AUTHOR INFORMATION

Corresponding Authors

Yves F. Dufrêne − *Institute of Life Sciences, Université Catholique de Louvain, Louvain-la-Neuve B-1348, Belgium;* orcid.org/0000-0002-7289-4248; Email: yves.dufrene@uclouvain.be

Joan A. Geoghegan − *Institute of Microbiology and Infection, University of Birmingham, Birmingham B15 2TT, U.K; Department of Microbes, Infection and Microbiomes, University of Birmingham, Birmingham B15 2TT, U.K;* Email: j.geoghegan@bham.ac.uk

Authors

Zhiyong Zheng − *Institute of Life Sciences, Université Catholique de Louvain, Louvain-la-Neuve B-1348, Belgium;* orcid.org/0000-0002-7276-7425

Manon Dechene-Tempier − *Institute of Life Sciences, Université Catholique de Louvain, Louvain-la-Neuve B-1348, Belgium*

Telmo O. Paiva − *Institute of Life Sciences, Université Catholique de Louvain, Louvain-la-Neuve B-1348, Belgium;* orcid.org/0000-0002-6524-3092

Can Wang − *Institute of Life Sciences, Université Catholique de Louvain, Louvain-la-Neuve B-1348, Belgium*

Sophie Dunn − *Institute of Microbiology and Infection, University of Birmingham, Birmingham B15 2TT, U.K; Department of Microbes, Infection and Microbiomes, University of Birmingham, Birmingham B15 2TT, U.K*

Julianne Clowry − *Clinical Medicine, Trinity College Dublin, Dublin D12N512, Ireland; Department of Dermatology, National Children's Research Centre, Children's Health Ireland at Crumlin, Dublin D12N512, Ireland*

Alan D. Irvine − *Clinical Medicine, Trinity College Dublin, Dublin D12N512, Ireland; Department of Dermatology, National Children's Research Centre, Children's Health Ireland at Crumlin, Dublin D12N512, Ireland*

Complete contact information is available at: https://pubs.acs.org/10.1021/acsnano.5c21776

Author Contributions

#Z.Z. and M.D.-T. contributed equally to this work. Z.Z., M.D.T., T.O.P., C.W., S.D., J.C., A.D.I, J.A.G., and Y.F.D. designed the experiments. Z.Z. and C.W. performed SCFS analyses. Z.Z. performed the Fg SMFS experiments. M.D.T. and T.O.P. performed the Fn SMFS experiments. Z.Z., M.D.T., T.O.P., C.W., J.A.G., and Y.F.D. analyzed the data. Z.Z., M.D.T., T.O.P., J.A.G., and Y.F.D. cowrote the paper with scientific interpretations, comments and edits from all

https://doi.org/10.1021/acsnano.5c21776
ACS Nano 2026, 20, 7279−7290

authors. All authors have given approval to the final version of the manuscript.

Notes

The authors declare no competing financial interest.

■ ACKNOWLEDGMENTS

Work at the UCLouvain was supported by "Actions de Recherche Concertées" funding and the National Fund for Scientific Research (FNRS). Y.F.D. is a Research Director at the FNRS. Z.Z. is a postdoctoral researcher at the FNRS. Work at the University of Birmingham was supported by a project grant from the British Skin Foundation (017/S/20).

■ REFERENCES

(1) David, M. Z.; Daum, R. S. Community-associated methicillin-resistant *Staphylococcus aureus*: Epidemiology and clinical consequences of an emerging epidemic. *Clin. Microbiol. Rev.* **2010**, *23*, 616−687.
(2) Feuillie, C.; Vitry, P.; McAleer, M. A.; Kezic, S.; Irvine, A. D.; Geoghegan, J. A.; Dufrêne, Y. F. Adhesion of *Staphylococcus aureus* to corneocytes from atopic dermatitis patients is controlled by natural moisturizing factor levels. *mBio* **2018**, *9*, e01184−18.
(3) Geoghegan, J. A.; Irvine, A. D.; Foster, T. J. *Staphylococcus aureus* and atopic dermatitis: A complex and evolving relationship. *Trends Microbiol.* **2018**, *26*, 484−497.
(4) Langan, S. M.; Irvine, A. D.; Weidinger, S. Atopic dermatitis. *Lancet* **2020**, *396*, 345−360.
(5) Towell, A. M.; Feuillie, C.; Vitry, P.; Da Costa, T. M.; Mathelié-Guinlet, M.; Kezic, S.; Fleury, O. M.; McAleer, M. A.; Dufrêne, Y. F.; Irvine, A. D.; Geoghegan, J. A. *Staphylococcus aureus* binds to the N-terminal region of corneodesmosin to adhere to the stratum corneum in atopic dermatitis. *Proc. Natl. Acad. Sci. U. S. A.* **2021**, *118*, No. e2014444118.
(6) da Costa, T. M.; Viljoen, A.; Towell, A. M.; Dufrêne, Y. F.; Geoghegan, J. A. Fibronectin binding protein B binds to loricrin and promotes corneocyte adhesion by *Staphylococcus aureus*. *Nat. Commun.* **2022**, *13*, 2517.
(7) Cho, S.-H.; Strickland, I.; Boguniewicz, M.; Leung, D. Y. M. Fibronectin and fibrinogen contribute to the enhanced binding of Staphylococcus aureus to atopic skin. *J. Allergy Clin. Immunol.* **2001**, *108*, 269−274.
(8) Speziale, P.; Pietrocola, G. The multivalent role of fibronectin-binding proteins A and B (FnBPA and FnBPB) of *Staphylococcus aureus* in host infections. *Front. Microbiol.* **2020**, *11*, 2054.
(9) Foster, T. J.; Geoghegan, J. A.; Ganesh, V. K.; Höök, M. Adhesion, invasion and evasion: the many functions of the surface proteins of *Staphylococcus aureus*. *Nat. Rev. Microbiol.* **2014**, *12*, 49−62.
(10) Paiva, T. O.; Viljoen, A.; da Costa, T. M.; Geoghegan, J. A.; Dufrêne, Y. F. Interaction of the *Staphylococcus aureus* surface protein FnBPB with corneodesmosin involves two distinct, extremely strong bonds. *ACS Nanosci. Au* **2023**, *3*, 58−66.
(11) Bao, L.; Mohan, G. C.; Alexander, J. B.; Doo, C.; Shen, K.; Bao, J.; Chan, L. S. A molecular mechanism for IL-4 suppression of loricrin transcription in epidermal keratinocytes: implication for atopic dermatitis pathogenesis. *Innate Immun.* **2017**, *23*, 641−647.
(12) Riethmuller, C.; McAleer, M. A.; Koppes, S. A.; Abdayem, R.; Franz, J.; Haftek, M.; Campbell, L. E.; MacCallum, S. F.; McLean, W. H. I.; Irvine, A. D.; Kezic, S. Filaggrin breakdown products determine corneocyte conformation in patients with atopic dermatitis. *J. Allergy Clin. Immunol.* **2015**, *136*, 1573−1580.e2.
(13) Kim, B. E.; Leung, D. Y. M.; Boguniewicz, M.; Howell, M. D. Loricrin and involucrin expression is down-regulated by Th2 cytokines through STAT-6. *Clin. Immunol.* **2008**, *126*, 332−337.
(14) Furue, M. Regulation of filaggrin, loricrin, and involucrin by IL-4, IL-13, IL-17A, IL-22, AHR, and NRF2: Pathogenic implications in atopic dermatitis. *Int. J. Mol. Sci.* **2020**, *21*, 5382.
(15) Leung, D. Y. M.; Bissonnette, R.; Kreimer, S.; Berdyshev, E.; Bafna, S.; Lyubchenko, T.; Richers, B. N.; Garcia, S.; Ramirez-Gama, M.; Hall, C. F.; Xiao, O.; Taylor, P.; Boguniewicz, M.; Levit, N. A.; Agueusop, I.; Zhang, A.; Goleva, E. Dupilumab inhibits vascular leakage of blood proteins into atopic dermatitis skin. *J. Allergy Clin. Immunol.: Pract.* **2023**, *11*, 1421−1428.
(16) Herrick, S.; Blanc-Brude, O.; Gray, A.; Laurent, G. Fibrinogen. *Int. J. Biochem. Cell Biol.* **1999**, *31*, 741−746.
(17) Adamczyk, Z.; Cichocki, B.; Ekiel-Jeżewska, M. L.; Słowicka, A.; Wajnryb, E.; Wasilewska, M. Fibrinogen conformations and charge in electrolyte solutions derived from DLS and dynamic viscosity measurements. *J. Colloid Interface Sci.* **2012**, *385*, 244−257.
(18) Milles, L. F.; Schulten, K.; Gaub, H. E.; Bernardi, R. C. Molecular mechanism of extreme mechanostability in a pathogen adhesin. *Science* **2018**, *359*, 1527−1533.
(19) Ponnuraj, K.; Bowden, M. G.; Davis, S.; Gurusiddappa, S.; Moore, D.; Choe, D.; Xu, Y.; Hook, M.; Narayana, S. V. L. A "dock, lock, and latch" structural model for a staphylococcal adhesin binding to fibrinogen. *Cell* **2003**, *115*, 217−228.
(20) Herman-Bausier, P.; Labate, C.; Towell, A. M.; Derclaye, S.; Geoghegan, J. A.; Dufrêne, Y. F. *Staphylococcus aureus* clumping factor A is a force-sensitive molecular switch that activates bacterial adhesion. *Proc. Natl. Acad. Sci. U. S. A.* **2018**, *115*, 5564−5569.
(21) Mathelié-Guinlet, M.; Viela, F.; Pietrocola, G.; Speziale, P.; Alsteens, D.; Dufrêne, Y. F. Force-clamp spectroscopy identifies a catch bond mechanism in a Gram-positive pathogen. *Nat. Commun.* **2020**, *11*.
(22) Viela, F.; Mathelié-Guinlet, M.; Pietrocola, G.; Speziale, P.; Dufrêne Yves, F. The molecular complex between staphylococcal adhesin SpsD and fibronectin sustains mechanical forces in the nanonewton range. *mBio* **2020**, *11*..
(23) Burke, F. M.; Di Poto, A.; Speziale, P.; Foster, T. J. The A domain of fibronectin-binding protein B of *Staphylococcus aureus* contains a novel fibronectin binding site. *FEBS J.* **2011**, *278*, 2359−2371.
(24) Burke, F. M.; McCormack, N.; Rindi, S.; Speziale, P.; Foster, T. J. Fibronectin-binding protein B variation in *Staphylococcus aureus*. *BMC Microbiol.* **2010**, *10*, 160.
(25) Erickson, H. P.; Carrell, N.; McDonagh, J. Fibronectin molecule visualized in electron microscopy: a long, thin, flexible strand. *J. Cell Biol.* **1981**, *91*, 673−678.
(26) Oberhauser, A. F.; Badilla-Fernandez, C.; Carrion-Vazquez, M.; Fernandez, J. M. The mechanical hierarchies of fibronectin observed with single-molecule AFM. *J. Mol. Biol.* **2002**, *319*, 433−447.
(27) Oberdörfer, Y.; Fuchs, H.; Janshoff, A. Conformational analysis of native fibronectin by means of force spectroscopy. *Langmuir* **2000**, *16*, 9955−9958.
(28) Oberdörfer, Y.; Schrot, S.; Fuchs, H.; Galinski, E.; Janshoff, A.; Oberdörfer, Y. Impact of compatible solutes on the mechanical properties of fibronectin: a single molecule analysis. *Phys. Chem. Chem. Phys.* **2003**, *5*, 1876−1881.
(29) Foster, T. J. The remarkably multifunctional fibronectin binding proteins of *Staphylococcus aureus*. *Eur. J. Clin. Microbiol. Infect. Dis.* **2016**, *35*, 1923−1931.
(30) Schwarz-Linek, U.; Werner, J. M.; Pickford, A. R.; Gurusiddappa, S.; Kim, J. H.; Pilka, E. S.; Briggs, J. A. G.; Gough, T. S.; Höök, M.; Campbell, I. D.; Potts, J. R. Pathogenic bacteria attach to human fibronectin through a tandem β-zipper. *Nature* **2003**, *423*, 177−181.
(31) Yongsunthon, R.; Fowler, V. G.; Lower, B. H.; Vellano, F. P.; Alexander, E.; Reller, L. B.; Corey, G. R.; Lower, S. K. Correlation between fundamental binding forces and clinical prognosis of *Staphylococcus aureus* infections of medical implants. *Langmuir* **2007**, *23*, 2289−2292.
(32) Buck, A. W.; Fowler, V. G.; Yongsunthon, R.; Liu, J.; DiBartola, A. C.; Que, Y.-A.; Moreillon, P.; Lower, S. K. Bonds between fibronectin and fibronectin-binding proteins on *Staphylococcus aureus* and *Lactococcus lactis*. *Langmuir* **2010**, *26*, 10764−10770.

https://doi.org/10.1021/acsnano.5c21776
ACS Nano 2026, 20, 7279−7290

(33) Stemberk, V.; Jones, R. P. O.; Moroz, O.; Atkin, K. E.; Edwards, A. M.; Turkenburg, J. P.; Leech, A. P.; Massey, R. C.; Potts, J. R. Evidence for steric regulation of fibrinogen binding to *Staphylococcus aureus* fibronectin-binding protein A (FnBPA). *J. Biol. Chem.* **2014**, *289*, 12842−12851.
(34) Viljoen, A.; Mathelié-Guinlet, M.; Ray, A.; Strohmeyer, N.; Oh, Y. J.; Hinterdorfer, P.; Müller, D. J.; Alsteens, D.; Dufrêne, Y. F. Force spectroscopy of single cells using atomic force microscopy. *Nat. Rev. Methods Primers* **2021**, *1*.
(35) Beaussart, A.; El-Kirat-Chatel, S.; Sullan, R. M. A.; Alsteens, D.; Herman, P.; Derclaye, S.; Dufrêne, Y. F. Quantifying the forces guiding microbial cell adhesion using single-cell force spectroscopy. *Nat. Protoc.* **2014**, *9*, 1049−1055.
(36) Herman, P.; El-Kirat-Chatel, S.; Beaussart, A.; Geoghegan, J. A.; Foster, T. J.; Dufrêne, Y. F. The binding force of the staphylococcal adhesin SdrG is remarkably strong. *Mol. Microbiol.* **2014**, *93*, 356−368.
(37) Dufrêne, Y. F.; Martínez-Martín, D.; Medalsy, I.; Alsteens, D.; Müller, D. J. Multiparametric imaging of biological systems by force-distance curve−based AFM. *Nat. Methods* **2013**, *10*, 847−854.
(38) Mills, K. B.; Maciag, J. J.; Wang, C.; Crawford, J. A.; Enroth, T. J.; Keim, K. C.; Dufrêne, Y. F.; Robinson, D. A.; Fey, P. D.; Herr, A. B.; Horswill, A. R. Staphylococcus aureus skin colonization is mediated by SasG lectin variation. *Cell Rep.* **2024**, *43*, 114022.
(39) Foster, T. J. Surface proteins of *Staphylococcus aureus*. *Microbiol. Spectrum* **2019**, *7*, 7.4.2−2018.
(40) Herman-Bausier, P.; Pietrocola, G.; Foster, T. J.; Speziale, P.; Dufrêne, Y. F. Fibrinogen activates the capture of human plasminogen by staphylococcal fibronectin-binding proteins. *mBio* **2017**, *8*, No. e01067.
(41) Wang, C.; Paiva, T. O.; Motta, C.; Speziale, P.; Pietrocola, G.; Dufrêne, Y. F. Catch bond-mediated adhesion drives *Staphylococcus aureus* host cell invasion. *Nano Lett.* **2023**, *23*, 5297−5306.
(42) Herman-Bausier, P.; Dufrêne, Y. F. Force matters in hospital-acquired infections. *Science* **2018**, *359*, 1464−1465.
(43) Prystopiuk, V.; Feuillie, C.; Herman-Bausier, P.; Viela, F.; Alsteens, D.; Pietrocola, G.; Speziale, P.; Dufrêne, Y. F. Mechanical forces guiding *Staphylococcus aureus* cellular invasion. *ACS Nano* **2018**, *12*, 3609−3622.
(44) Otto, M. Physical stress and bacterial colonization. *FEMS Microbiol. Rev.* **2014**, *38*, 1250−1270.
(45) Vitry, P.; Valotteau, C.; Feuillie, C.; Bernard, S.; Alsteens, D.; Geoghegan, J. A.; Dufrêne, Y. F. Force-induced strengthening of the interaction between *Staphylococcus aureus* clumping factor B and loricrin. *mBio* **2017**, *8*, No. e01748.
(46) Paiva, T. O.; Geoghegan, J. A.; Dufrêne, Y. F. High-force catch bonds between the *Staphylococcus aureus* surface protein SdrE and complement regulator factor H drive immune evasion. *Commun. Biol.* **2023**, *6*.
(47) Evans, E.; Ritchie, K. Dynamic strength of molecular adhesion bonds. *Biophys. J.* **1997**, *72*, 1541−1555.
(48) Casillas-Ituarte, N. N.; DiBartola, A. C.; Broughton, M. J.; Pérez-Guzmán, L.; Wheeler, R. M.; Ibaraki, M.; Lower, B. A.; Dunn, J. A.; Lower, B. H.; Fowler, V. G.; Hüük, M.; McIntyre, L. M.; Lower, S. K.; Sharma-Kuinkel, B. K. Fibrinogen binding is affected by amino acid substitutions in C-terminal repeat region of fibronectin binding protein A. *Sci. Rep.* **2019**, *9*, 11619.
(49) Chantraine, C.; Gomes, P. S. F. C.; Mathelié-Guinlet, M.; Gomes, D. E. B.; Zheng, Z.; Clowry, J.; Turley, M. B.; Irvine, A. D.; Geoghegan, J. A.; Bernardi, R. C.; Dufrêne, Y. F. Ultrastrong Staphylococcus aureus adhesion to human skin: Calcium as a key regulator of noncovalent interactions. *Sci. Adv.* **2025**, *11*, No. eadu7457.
(50) McAleer, M. A.; Jakasa, I.; Hurault, G.; Sarvari, P.; McLean, W. H. I.; Tanaka, R. J.; Kezic, S.; Irvine, A. D. Systemic and stratum corneum biomarkers of severity in infant atopic dermatitis include markers of innate and T helper cell-related immunity and angiogenesis. *Br. J. Dermatol.* **2019**, *180*, 586−596.
(51) Paiva, T. O.; Speziale, P.; Dufrêne, Y. F. Force nanoscopy demonstrates stress-activated adhesion between *Staphylococcus aureus* iron-regulated surface determinant protein B and host toll-like receptor 4. *ACS Nano* **2025**, *19*, 989−998.
(52) Wang, C.; Paiva, T. O.; Speziale, P.; Dufrêne, Y. F. Nanomechanics of CCN1-mediated *Staphylococcus aureus* phagocytosis. *Nano Lett.* **2024**, *24*, 8567−8574.
(53) Viljoen, A.; Vercellone, A.; Chimen, M.; Gaibelet, G.; Mazères, S.; Nigou, J.; Dufrêne, Y. F. Nanoscale clustering of mycobacterial ligands and DC-SIGN host receptors are key determinants for pathogen recognition. *Sci. Adv.* **2023**, *9*, No. eadf9498.
(54) Sader, J. E.; Larson, I.; Mulvaney, P.; White, L. R. Method for the calibration of atomic force microscope cantilevers. *Rev. Sci. Instrum.* **1995**, *66*, 3789−3798.

https://doi.org/10.1021/acsnano.5c21776
ACS Nano 2026, 20, 7279−7290